ACS APPLIED ELECTRONIC MATERIALS

Article

Cite This: ACS Appl. Electron. Mater. 2019, 1, 1873−1880

pubs.acs.org/acsaelm

Detecting Minute Chemical Vapors via Chemical Interactions between Analyte and Fluorinated Thiophene−Isoindigo Conjugated Polymer Transistor

Chun-Fu Lu,[†] Song-Fu Liao,[†,‡] Iu-Fan Chen,[†] Chin-Ti Chen,[‡] Chi-Yang Chao,[†] and Wei-Fang Su*[,†]

[†]Department of Materials Science and Engineering, National Taiwan University, Taipei 10617, Taiwan

[‡]Institute of Chemistry, Academia Sinica, No. 128, Academia Road, Sec. 3, Taipei 11529, Taiwan

Supporting Information

ABSTRACT: Detecting and discriminating chemical vapors are essential for environmental monitoring and medical diagnostics. In this study, highly sensitive chemical vapor sensors fabricated from fluorinated thiophene−isoindigo donor−acceptor conjugated polymers are realized through understanding the interaction of the fluorine functional group and different chemical vapors. The polymers possess the merits of facile synthesis for high quality materials, good field-effect transistor performance, and stability in air and humid environments. The transistor exhibits extremely high detecting capability for minute chemical vapor down to the ppb range. The detecting sensitivity of the transistor depends on the chemical structure of the polymer and the nature of analytes. Polar molecules such as amines with potential hydrogen bond donor can adsorb in close vicinity to conducting channels due to the formation of a hydrogen bond with fluorine atoms, enhancing the sensitivity significantly. Chemical vapors such as acetone and xylene interacting with the polymers via dipolar and van der Waals forces, respectively, have to accumulate sufficient amounts in the polymer films or at the dielectric interface. Through understanding functional group−analyte interactions, polymers can be designed for multiparameter sensing, paving ways toward ultrasensitive sensors and accurate discrimination of different kinds of chemical vapors.

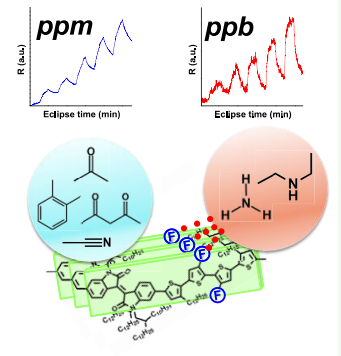

KEYWORDS: *chemical sensor, polymer, fluorination, functional group, field-effect transistor*

INTRODUCTION

Chemical vapor sensing plays an essential part in the present and ongoing development of diagnostic technologies for noninvasive medical evaluation and alarms for the possible presence of hazardous chemicals.[1−3] Health-related chemical vapors widely investigated in sensor development include alcohols, amines, ketones, nitrogen oxides, phosphonates, and other volatile organic compounds. Electrical transduced chemical vapor sensors have been developed from active materials like metal oxides, organic small molecules, carbon nanotubes, graphene, and polymers. Recent progress in polymer field-effect transistors (FETs), including the improvement of device performance and storage/operating stability, promotes the studies in the aspect of chemical vapor sensing. The semiconducting polymers are considered outperforming metal oxides and organic small molecules due to their advantages of low operation temperature, tunable chemical structures, and excellent film integrity by the solution process.

Promoting the interaction between analytes and charge transport channels is widely explored to improve sensitivity and selectivity of chemical vapors sensing by polymer FETs.[4] Katz et al.[5] introduced an ammonia receptor molecule, tris(pentafluorophenyl)borane, which interacts with ammonia via strong B−N Lewis adduct formation. Zhang et al.[6] incorporated a carboxyl group at polymer side chains to chemically react with ammonia. Although the approach of sensing by chemical reaction greatly improves the sensitivity of the sensor, the sensor suffers from poor recovery due to the strong analyte−polymer interaction. The recovery from either hydrogen bond formation or dipolar interaction with analytes is more efficient and is beneficial for chemical vapor detection. Noh and co-workers[7] reported improved sensitivity to ammonia by utilizing hydrogen bonding between ammonia and fluorine atoms incorporated in both conjugated polymer and dielectrics. The hydrogen bonding between ammonia and fluorine atoms has been confirmed by cyclic voltammetry (CV) and NMR. Few polymer FET sensors have been reported for analytes like acetone and xylene because they have a rather weak interaction with the conducting channels of the FET sensor. In addition to understanding the interaction between the sensing functional group of the polymer and analytes, it is also important to investigate other influences of the functional group, such as the alignment of the sensing

Received: June 23, 2019
Accepted: August 22, 2019
Published: August 22, 2019

DOI: 10.1021/acsaelm.9b00396
ACS Appl. Electron. Mater. 2019, 1, 1873−1880

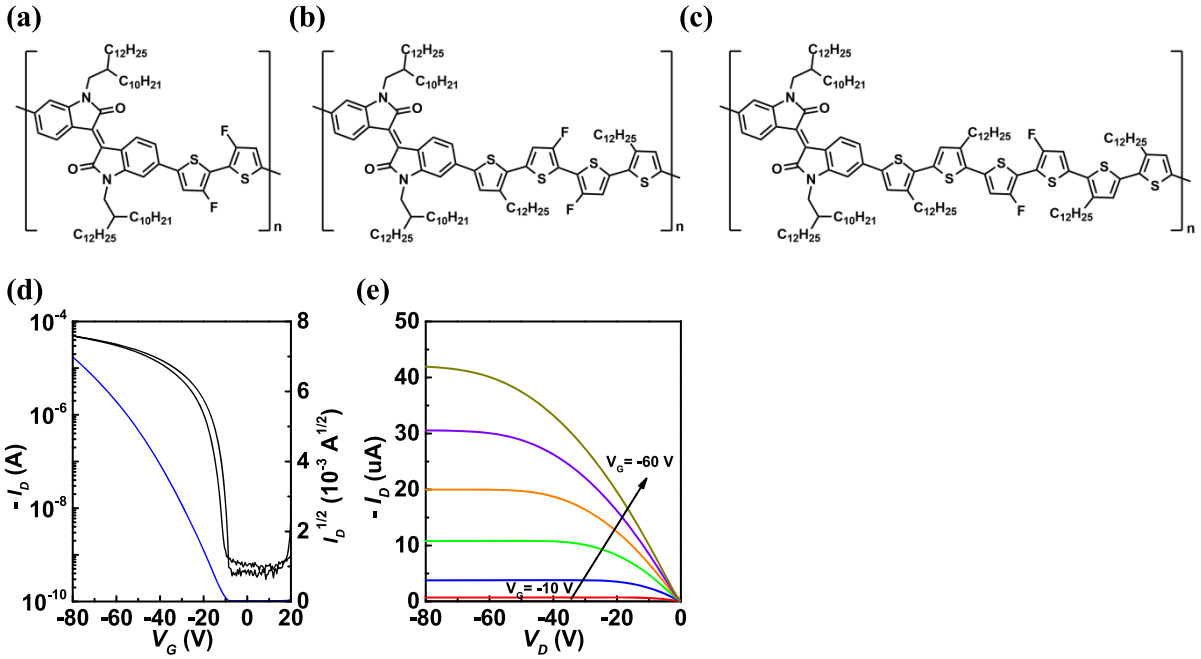

Figure 1. Chemical structures of (a) P2TIF, (b) P4TIF, and (c) P6TIF. Representative (d) transfer characteristics and (e) output curves of a P4TIF FET.

polymer in FET sensor, which has a profound influence on FET, both transistor and sensing performances.

Donor (D)−acceptor (A) π-conjugated polymers have hitherto been the most promising polymers for building high-sensitivity chemical vapor sensors because of the versatile chemical structures, good electrical stability in air, and outstanding FET performance. With regard to the functional group, fluorination has been employed to improve charge transport properties and device stability for various D−A copolymers.[8−11] Therefore, incorporating fluorine atoms in D−A π-conjugated polymers can lead to potential sensing materials for ammonia and acetone. Besides functionality, various factors in a polymer FET device can influence the chemical vapors sensing, including polymer packing order,[12] thin film morphologies of polymers,[13,14] polymer film thickness,[15] and dielectric materials[16] in the device. Isoindigo is an ideal electron accepting unit to synthesize D−A π-conjugated polymers as active sensing materials for three reasons. (1) Isoindigo is a sustainable chemical which is extractable from plants.[17] (2) The chemical structure of isoindigo enables functionalization which is not available for other widely explored acceptor moieties such as pyrrolo[3,4-*c*]pyrrole-1,4-dione (DPP) or thieno[3,4-*c*]pyrrole-4,6-dione (TPD). (3) The two lactam rings in isoindigo leads to planar polymer backbone and long conjugation length,[18] which are both beneficial for charge transport in FET. Thus, isoindigo-based copolymers possess versatile functionality in both donor and acceptor segments and have eco-friendly sources for future production.

In this study, we have synthesized a series of carefully designed D−A copolymers with different contents of fluorine atoms to investigate the influence of fluorine atoms in chemical vapor sensing. Three polymers, namely P2TIF, P4TIF, and P6TIF, consist of an isoindigo (I) electron accepting unit and two fluorine atoms in the electron donating segments of bithiophene (2T), quaterthiophene (4T), and sexithiophene (6T) in one repeating unit of the copolymers. An even number of thiophene segments results in more edge-on polymer packing and high crystallinity.[12,19] The relationships among the chemical structure, transistor performance, and vapor sensing capability are systematically studied. We have demonstrated that the hole mobility of transistors, the device stability, and the sensitivity of sensors can be greatly enhanced by incorporating fluorine atoms on the thiophene unit of the polymer main chain. The P4TIF FET exhibits high hole mobility up to 0.49 cm^2 V^{-1} s^{-1}, over an order improvement than its unfluorinated counterpart. With regard to detection of chemical vapor, the hydrogen bond formed by the ammonia molecule and fluorine atoms enhances the detection sensitivity considerably while the acetone molecules are attached to the polymer without specific interaction with fluorine atoms. Our polymer FET sensors can differentiate various chemical vapors with low concentrations, such as 100 ppb for ammonia and 50 ppm for acetone gas, within 2 min in air.

RESULTS AND DISCUSSION

Synthesis and Electrical Properties of P*n*TIF. P*n*TIF polymers with different fluorine contents were used in this study to investigate the impact of fluorination, and their chemical structures are shown in Figure 1a−c. To achieve high purity, high degree of polymerization, and low molecular weight distributions (PDI), P*n*TIF polymers were polymerized by Stille coupling from trimethyltin-functionalized fluorinated bithiophene and the corresponding electron acceptor moiety. The isoindigo with null, two, and four flanked alkylated thiophenes were used as an electron acceptor moiety for P2TIF, P4TIF, and P6TIF, respectively. The atomic ratio of fluorine atoms in P2TIF, P4TIF, and P6TIF is 1.91:1.31:1.00. The detailed synthesis route and general method are included in the Supporting Information. The polymers with optimal FET performance have number-average molecular weights (M_n) of 109.6−156.1 kDa, and PDI are in the range of 1.35−1.60. Charge transport properties of P*n*TIF polymers were characterized by bottom-gate top-contact geometry FET

DOI: 10.1021/acsaelm.9b00396
ACS Appl. Electron. Mater. 2019, 1, 1873−1880

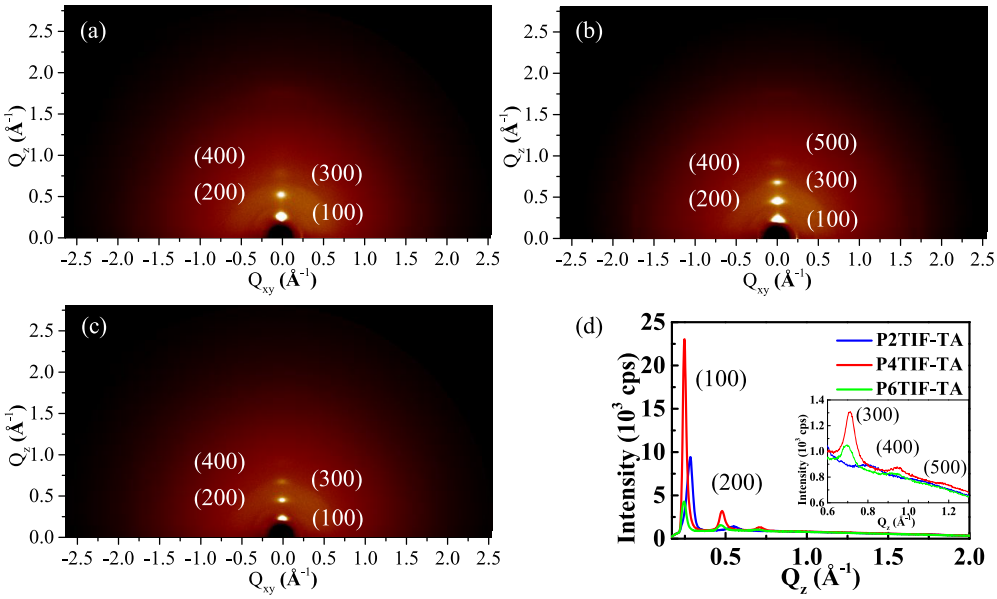

Figure 2. 2D grazing incidence wide-angle X-ray scattering (GIWAXS) images of (a) P2TIF, (b) P4TIF, and (c) P6TIF thin films. (d) 1D GIWAXS profiles of P2TIF, P4TIF, and P6TIF integrated along the out-of-plane direction. The inset shows the enlarged profiles to reveal (300) and (400) diffraction peaks. All films were annealed at respectively optimal temperatures in vacuum for an hour.

devices. All P*n*TIF polymers exhibit p-type transfer characteristics with negligible hysteresis and contact resistance. Figure 1d shows the representative I_D-V_G curve of a P4TIF FET measured in an ambient environment. The clear field effect can be observed from the output characteristics of a P4TIF FET in Figure 1e. The averaged mobilities of P*n*TIF FETs calculated from the I_D-V_G curves are 0.12, 0.41, and 0.065 cm^2 V^{-1} s^{-1}, respectively, with the highest value reaching up to 0.49 cm^2 V^{-1} s^{-1} from P4TIF FET. Table S1 summarizes the FET characteristics of P*n*TIF thin films.

Stable device performance in air and humid environments is a vital criterion for a high-sensitivity chemical vapor sensor. P*n*TIF FETs exhibit excellent stability not merely under ambient conditions but in high-humidity environments as well. All devices retain their transistor characteristics with at least 90% of their mobilities after storing in the environment of 40%, 85%, and 97.5% humidity for 120 days without encapsulation; details are included in Figure S4. The stable hole transport of P*n*TIF polymers might be accounted by their deep highest occupied molecular orbital (HOMO) energy levels, i.e., lower than −5.2 eV. The cyclic voltammetry-measured HOMO energy levels of P2TIF, P4TIF, and P6TIF are −5.69, −5.41, and −5.26 eV, respectively (Figure S5). The difluoro-substituted bithiophene segment in P*n*TIF polymers leads to their low-lying HOMO values. This phenomenon is also observed in the literature.[20−23] In the following investigation of chemical vapor sensing, dry air is used as carrier gas to avoid the slight but potential variation caused by moisture.

Morphologies of P*n*TIF Thin Films. In general, the sensitivity of a sensor is related to the incorporated functional groups, polymer crystallites, and surface morphology of active materials. To rationalize the effect of the fluorine content on the sensing ability, P*n*TIF should have similar surface morphology and polymer packing orientation. The morphologies of P*n*TIF thin films were examined by grazing incidence wide-angle X-ray scattering (GIWAXS) and atomic force microscope (AFM). As shown in Figure 2a−c, P*n*TIF thin films exhibit well-defined high order reflections along the Q_z direction, corresponding to edge-on packing lamella structure of polymers. Polymers with their alkyl side chains perpendicular to the silicon substrate are called "edge-on", which is beneficial for the charge transport in a FET device. The clear (400) reflections with small azimuthal angles indicate that the lamella structures in P*n*TIF thin films are of high crystallinity and well-ordered packing. The 1D GIWAXS patterns in Figure 2d were obtained through integrating the line cuts along the Q_z-axis. The crystallographic parameters for P2TIF, P4TIF, and P6TIF are summarized in Table S4. The second-order reflection peaks in the obtained 1D GIWAXS patterns are used to calculate the lamella spacing (d_{100}) of each polymer. P2TIF has smaller lamellae spacing (23.3 Å) comparing to P4TIF (26.4 Å) and P6TIF (26.5 Å). This result can be explained by the chemical structure of P*n*TIF. There are two alkyl side chains in a repeat unit of P2TIF while there are four and six alkyl side chains in a repeat unit of P4TIF and P6TIF, respectively. As polymer side chains take up considerable spacing between polymer main chains, P2TIF can pack closer than the other two polymers. The coherence lengths (L_C) can serve as a measure of the crystalline domain size in polymer thin films due to their polycrystalline nature. Calculated by Scherrer's equation, the coherence lengths of P2TIF, P4TIF, and P6TIF are 133, 175, and 173 Å, respectively. The L_C values of P4TIF and P6TIF indicate that their polymeric crystallites are of similar domain size. The surface morphologies of P*n*TIF thin films were examined by tapping mode AFM. The height and phase images are included in Figure S7. The P2TIF thin film consists of numerous bundles of fibers in the size ranging from 20 to 100 nm at the upmost layer. In contrast, P4TIF and P6TIF have the surface consisting of connected polymeric crystals without particular long-ranged structures. Therefore, the sensing results of P4TIF and P6TIF can be highly related to the only difference in fluorine content because they possess similar surface morphologies, crystalline sizes, and polymer packing.

DOI: 10.1021/acsaelm.9b00396
ACS Appl. Electron. Mater. 2019, 1, 1873−1880

Detection of Chemical Vapors. To investigate the effect of fluorine functional group on chemical vapors sensing, P*n*TIF FETs were exposed to various chemical vapors. Three kinds of chemical vapors were studied: high polar molecules with potential hydrogen bond formation, such as diethylamine (DEA) and ammonia; high polar molecules without potential hydrogen source for hydrogen bond formation, including acetonitrile (ACN) and acetylacetone (AA); and hydrophobic aromatic compounds like xylene. To reveal the effect of chemical vapors on charge transport characteristics, the drain currents of P*n*TIF films were recorded after exposure to chemical vapors of 5000 ppm for 20 min. We herein define an equilibrium response R_{eq} in the following equation:

$$R_{eq} = \frac{I_D(\text{air}) - I_D(\text{analyte})}{I_D(\text{air})} \quad (1)$$

where I_D(air) and I_D(analyte) are the drain current after exposing to air and analyte environment, respectively. Chemical structures of the investigated analytes and their sensing results are visualized in Figure 3a, and the calculated values are summarized in Figure S9. In the presence of ACN, P2TIF exhibits the largest R_{eq} of 0.63, followed by P4TIF (0.25) and P6TIF (0.09). The response magnitude of P*n*TIF to ACN is correlated to the fluorine content of the polymer, which can be accounted by the dipole−dipole interaction between ACN and fluorine atom. ACN molecules are attracted by the cyano−fluorine interaction to the polymer film, leading to the decrease in conductance. The other polar chemical vapor acetylacetone, however, induces different responses from P*n*TIF polymers. Without definite attractive force, AA can merely change the charge carrier transport characteristics by accumulating at the polymer/dielectric interface, which is more pronounced in polymers with lower mobility. Thus, the R_{eq} of P2TIF and P6TIF are larger than the R_{eq} of P4TIF, which possess the highest hole mobility among the three investigated polymers. Regardless of their polarity, chemical vapors influencing the semiconducting polymer by this method result in similar sensing responses. Xylene, an aromatic compound with low polarity, changes the electric field by physically adsorbing in the polymer film and at the polymer/dielectric interface. The equilibrium response of xylene is in similar trend of AA. By comparison, exposing to vapor of DEA or ammonia leads to tremendous changes in FET characteristics. All P*n*TIF FETs lose their semiconducting characteristics, and the drain currents are reduced to about 10^{-9} A after exposure to 0.5% DEA or ammonia in 20 min. Such enormous changes in the *I*−*V* response of a FET device suggest that P*n*TIF polymers have higher selectivity to DEA and ammonia than ACN, AA, and xylene. Also, the detection of DEA and ammonia in ppb level can be realized by using P*n*TIF FETs.

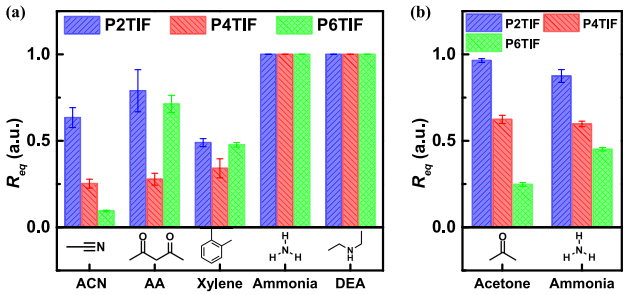

Figure 3. Sensing responses of P*n*TIF FETs to (a) 0.5% of acetonitrile (ACN), acetylacetone (AA), xylene, ammonia, and diethylamine (DEA) vapors in air for 20 min; (b) 500 ppm acetone and 50 ppm ammonia in air for 20 min.

To further investigate the influence of fluorine, P*n*TIF FETs were exposed to 50 ppm ammonia for a low-level doping without severe trapping of the conducting channels. Figure 3b shows the sensing response of P*n*TIF FETs to 50 ppm ammonia and 500 ppm acetone for comparison. The role of fluorine in sensing chemical vapors can be revealed by discerning the correlation between equilibrium response and fluorine content of the polymer. First-order correlation is assumed in the adsorption of the analytes and the resulting current change. The plot of equilibrium response and fluorine content of the polymer is included in Figure S9. Interestingly, the averaged ratio of equilibrium response to ammonia for P2TIF, P4TIF, and P6TIF is 1.94:1.32:1.00. The sensing response shows a linear correlation to fluorine content only when exposing to ammonia. This indicates that the sensitivity to ammonia can be enhanced by a potential hydrogen bond between fluorine atoms and ammonia. On the other hand, equilibrium responses to 500 ppm acetone increase with fluorine content, but no distinct correlation is observed. Also, the response to acetone decreases significantly with decreasing acetone concentration since acetone does not introduce vast amounts of traps in conducting channels. Choosing ammonia and acetone as representative chemical vapors has their

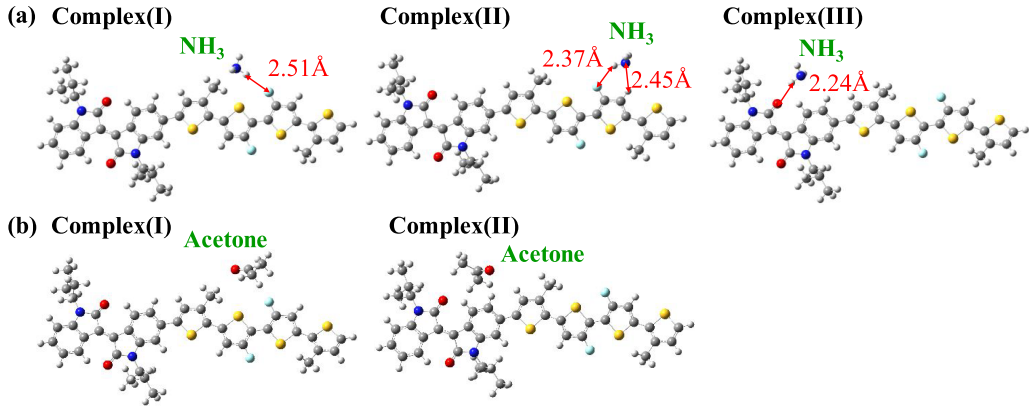

Figure 4. Optimized geometric structures of (a) 4TIF−ammonia complexes and (b) 4TIF−acetone complexes.

DOI: 10.1021/acsaelm.9b00396
ACS Appl. Electron. Mater. 2019, 1, 1873−1880

Table 1. DFT-Calculated HOMO/LUMO Energies of the 4TIF, 4TIF−Ammonia Complexes, and 4TIF−Acetone Complexes

		4TIF−ammonia			4TIF−acetone	
energy level	4TIF	case 1	case 2	case 3	case 1	case 2
LUMO [eV]	−2.777	−2.723	−2.762	−2.758	−2.730	−2.819
HOMO [eV]	−4.934	−4.881	−4.859	−4.878	−4.923	−4.872

biological significance in potential applications in biosensing and health care products. Ammonia, the simplest molecule of amines, is extensively studied because ammonia is a pathogenetic factor for Alzheimer's disease[24] and a potential biomarker for liver,[25] renal diseases,[3,26,27] asthma, and *Helicobacter pylori* infection.[28,29] On the other hand, acetone has been reported to possess potential association with diabetes mellitus,[30−34] a chronic disease increasing globally. Therefore, we further investigate the interaction of F−ammonia and F−acetone to uncover the role of fluorine in the detection of two highly interested chemical vapors.

Fluorine−Analyte Interactions. To correlate the polymer−analyte interactions and their sensing responses, density functional theory (DFT) was used to simulate the P*n*TIF−ammonia and P*n*TIF−acetone interactions. The geometry and electronic properties were estimated by the B3LYP functional using the 6-31** basis. 4TIF serves as the model monomer in the DFT calculation to simplify the computation complexity. Several 4TIF−ammonia complexes were investigated. There are three adsorption sites for ammonia molecules as depicted in Figure 4a. The interactions of C−FH−N−H_2, C−OH−N−H_2, and C−HNH_3 between 4TIF and ammonia decide the specific spatial arrangement of the ammonia molecule. A hydrogen bond formed between fluorine and ammonia has the strongest impact. When a NH_3 molecule is in close proximity to fluorine atoms, the NH_3 molecule moves to the position with one of its H atom aligning with fluorine. In addition, the thermodynamically favored distance between F and H is between 2.37 and 2.51 Å. Thus, the hydrogen bond formation between fluorine and ammonia can specifically attract ammonia to P*n*TIF polymers. In p-type FETs, the hole-injection barrier results from the energy difference between the work function of the metal electrode and HOMO energy level of the polymer. A higher negative gate voltage is required to open the hole channel when the hole-injection barrier increases. DFT-calculated energy levels of 4TIF, 4TIF−ammonia, and 4TIF−acetone complexes are summarized in Table 1. The HOMO energy levels of 4TIF increase after the adsorption of ammonia in all cases, leading to the increased hole-injection barrier. Thus, the threshold voltage shifts negatively after the intake of ammonia, as noted in the following experiments. The shifts in HOMO/LUMO energy levels are also observed in the literature due to the absorption of ammonia[7] and other chemical vapors.[35] In contrast, the 4TIF−acetone interaction differs from the hydrogen bond formation of 4TIF−ammonia. Acetone molecule does not locate at a fixed spatial position near 4TIF, and only a weak dipole−induced dipole interaction is found between the two molecules. Figure 4b depicts the two representative cases for the interaction of 4TIF−acetone without particular adsorption sites. Also, only complex(II) shows a lowered HOMO energy level while the HOMO energy level of complex(I) is similar to 4TIF. Thus, acetone molecules affect charge transport in P4TIF not by imposing effective traps but by perturbing the electric field near the conducting channels.

Real-Time Sensing of Minute Chemical Vapors. Encouraged by the positive correlation of fluorine content and ammonia sensing response, real-time sensing of ammonia was carried out. P*n*TIF FETs were exposed to minute concentration of ammonia ranging from 100 ppb to 3 ppm in air to test their lower detection range. We hereby define the sensing response by the measured drain currents changes as

$$R = \frac{I_D(0) - I_D(t)}{I_D(0)} \quad (2)$$

where $I_D(t)$ and $I_D(0)$ are the drain current at time t and the beginning of the measurement, respectively. The sensing responses of P*n*TIF are shown in Figure 5a. The response

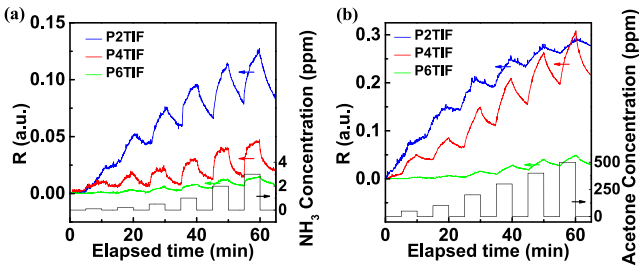

Figure 5. (a) Real-time sensing response of P*n*TIF FETs to various concentrations of ammonia ranging from 100 ppb to 3 ppm. (b) Sensing response of P*n*TIF FETs to various concentrations of acetone ranging from 50 to 500 ppm.

magnitude of P*n*TIF to ammonia is in the same order as the fluorine contents of the conjugated polymer, which is in the order of P2TIF, P4TIF, and P6TIF. The responses of P2TIF and P4TIF are easily 3 times larger than that of P6TIF; the high fluorine contents of P2TIF and P4TIF account for such a large difference in response magnitude. With the highest fluorine content among the investigated polymers, P2TIF responds drastically when exposed to ammonia. However, the sensing performance of P2TIF is impaired by baseline drift upon the intake of ammonia. Ammonia molecules are adsorbed specifically on difluoro-substituted bithiophenes via a hydrogen bond. The observed baseline drift and the resulting slow recovery are accounted by the chemical structure of P2TIF, i.e., high fluorine content and no additional thiophene spacer. Thermal properties of P*n*TIF polymers were analyzed by thermogravimetric analysis (TGA) and differential scanning calorimetry (DSC) analysis, and their results are included in Figure S10. P2TIF has no melting point observed up to 350 °C, which confirms that the chemical structure of P2TIF leads to a rigid polymer main chain. Thus, thermal annealing is less effective on P2TIF polymer films, and there are more defects in the polymer film, causing the observed baseline drift. Despite suffering from the low detrapping rate, P2TIF can detect 200 ppb ammonia in air within 2 min. On the other hand, P4TIF and P6TIF FETs can recover from the trapping by ammonia effectively. Also, thermal treatment can greatly improve the packing order of P4TIF and P6TIF because of

DOI: 10.1021/acsaelm.9b00396
ACS Appl. Electron. Mater. 2019, 1, 1873−1880

their softer polymer main chains than P2TIF. P4TIF and P6TIF have melting point of 297.2 and 252.2 °C, respectively. Drift currents in P4TIF and P6TIF FETs are negligible. P4TIF can detect 100 ppb ammonia in 1 min while P6TIF can respond to 200 ppb ammonia in 2 min. Note that the sensing materials are plain P*n*TIF polymer films without special film structures and additional receptor molecules in the films. Successful detection of 100 ppb ammonia is among the best in polymer FET-based ammonia sensors. Figure 5b shows the in-situ response of P*n*TIF FET to acetone vapor ranged from 50 to 500 ppm in air. P4TIF FET show a large response to 50 ppm acetone in 2 min while both P2TIF and P6TIF are eligible to detect 100 and 200 ppm acetone, respectively. To the best of our knowledge, this is among the best sensitivity for acetone achieved by polymer FET-based sensors.

CONCLUSIONS

In summary, we have explored the functionalized conjugated polymers in detection of different chemical vapors ranging from polar to nonpolar molecules. Polar chemical vapors are more sensitive than the nonpolar vapors. We further studied the role of fluorine atoms for sensing various chemical vapors by studying the polymer−analytes interaction via the DFT calculation. Polar molecules with potential sites for hydrogen bond formation, such as ammonia, can enhance their adsorption and thus in close vicinity to conducting channels by forming hydrogen bonds with fluorine atoms. By exploring the effect, 100 ppb ammonia vapor can be easily detected by P4TIF FET without additional receptors or specific film structures. For chemical vapors without specific binding with fluorine, they are detected via changing electrical field near charge carrier channels of conjugated polymers. Analyte concentration in the ppm level is required for the accumulation of analytes in the polymer film or polymer/dielectric interface mostly by diffusion. P*n*TIF polymers can detect 50 ppm acetone without additional receptors or nanostructures. Through understanding the interaction between analytes and functional groups in polymers, materials with careful design can realize ultrasensitive sensors and accurate differentiation of different kinds of chemical vapors.

EXPERIMENTAL METHODS

Materials. P*n*TIF polymers were synthesized via Stille coupling from fluorinated bithiophene and the respective isoindigo moiety with or without additional alkylated thiophenes. The synthesis route and general method were included in the Supporting Information. Detailed synthesis methods and characterization were discussed in our parallel work[36] using P*n*TIF polymers as active layers in polymer photovoltaics. The P*n*TIF polymers used in this study have number-average molecular weight (M_n) and molecular weight distribution (PDI) in the ranges of 109.6−156.1 kDa and 1.35−1.60, respectively. These values were determined by gel permeation chromatography (GPC) at 50 °C by using chloroform as eluent, and monodisperse polystyrene was used to calibrate the results. All chemical reagents purchased from suppliers were used as received unless otherwise mentioned.

Device Fabrication. Bottom-gate top-contact geometry was adopted for the polymer field-effect transistors in this work. Highly doped n-type silicon with 300 nm thermal oxide was modified with a self-assembled monolayer (SAM). The procedure was as follows. The silicon wafer was first cleaned by the oxygen plasma for 15 min, and a solution of 3.0 mM trimethoxy(octadecyl)silane in anhydrous trichloroethylene was spin-cast on the wafer. The OTS-covered wafer was then treated with ammonia vapor for 12 h and cleaned with toluene, ethanol, and acetone by an ultrasonicator. The P*n*TIF polymers were spin-cast from chloroform solution (0.10 wt %) onto the OTS-modified substrates at 800 rpm for 1 min in a nitrogen environment. P*n*TIF thin films were then annealed in vacuum for an hour, and the polymer films were slowly cooled to room temperature. The optimal annealing temperatures for P2TIF, P4TIF, and P6TIF were 240, 240, and 210 °C, respectively. The 100 nm Au was thermally evaporated on polymer films through shadow masks as source/drain electrodes, which featured the channel length (L) of 100 μm and the channel width (W) of 1 mm.

Measurement. A precision source/measurement unit (B2912A, Keysight, US) was used to measure the electrical properties of the P*n*TIF FETs in addition to a probe station or a temperature-controlled stage (Linkam Scientific, UK). The mobility (μ) at saturation region was calculated from the equation

$$\mu_{sat} = \frac{\left(\frac{d\sqrt{I_{SD}}}{dV_{SG}}\right)^2}{\frac{1}{2}C_i\frac{W}{L}} \quad (3)$$

where I_{SD} is the source-drain current, V_{SG} is the source-gate voltage, W and L are the channel width and length, and C_i is the dielectric constant of SiO_2 (10^{-4} F m^{-2}). The environmental stability of P*n*TIF FETs was conducted by placing the devices in ambient environments with different humidity of 40, 70, 85, and 97.5% RH. For 40% RH, the devices were placed in the lab without sealing. The tests for other humidity level followed the ASTM standard practice for maintain constant relative humidity by means of aqueous solutions.[37] The samples were placed in a container of 866 cm^3 with 40 mL of saturated aqueous potassium iodide, potassium chloride, and potassium sulfate solutions for 70, 85, and 97.5% RH, respectively. The GIWAXS analysis was performed at the National Synchrotron Radiation Research Center (NSRRC) in Taiwan, using beamline 13A and 17A. The P*n*TIF thin films for GIWAXS measurements were prepared as described above without the top contact electrodes. The thin films were carefully aligned and adjusted to afford X-ray incident angle of 0.2° for each measurement. The tapping mode of atomic force microscopy (OMV-NTSC, Bruker) was used to probe the surface morphology of polymer thin films. The thicknesses of P*n*TIF thin films were measured by AFM. Part of the polymer film was scratched off the substrate before the measurement. The average film thicknesses of P2TIF, P4TIF, and P6TIF from nine samples were 22.0, 20.1, and 14.9 nm, respectively. Cyclic voltammetry was performed by an electrochemical analyzer (CH Instruments CHI620A, US) to calculate energy levels of P*n*TIF. Polymer films were formed directly on the glassy carbon standard working electrode and then measured against the Ag/Ag$^+$ reference electrode with the internal standard of ferrocene/ferrocenium (Fc/Fc$^+$) in 0.1 M tetrabutylammonium hexafluorophosphate ($TBAPF_6$)−acetonitrile solution. The scan rate of cyclic voltammetry is 100 mV s^{-1}. For ammonia and acetone sensors, the FETs were measured in an airtight sealing temperature controlled stage. Mass flow controllers (Alicat, US) were used to prepare various concentrations of ammonia environments by diluting ammonia/air standard of 50 ppm with carrier gas (dry air). The prepared gas was concurrently transported into the temperature-controlled stage, where the sensor operated at 25 °C and 1 atm. The detection of acetone was conducted in a similar procedure with the acetone environments diluting from acetone/air standard of 500 ppm. For other chemical vapors, the chemicals were evaporated in a custom-made chamber under reduced pressure and then mixed with dry air to reach 1 atm. The chemical vapors were circulated in a closed system for 30 min before they were transported to the sensor chamber by micropumps at the flow rate of 10 cm^3/s. To date, chemical vapors that can be detected by polymer FETs at few ppm level are limited to vapors such as NO_2, H_2S, NH_3, and some amines. To study the response of P*n*TIF FETs for different chemical vapors, 0.5% (5000 ppm) TEA, ACN, AA, and xylene were used to show the selectivity of P*n*TIF. P*n*TIF FETs were exposed to these chemical vapors for 20 min before measurement to reach the equilibrium of the adsorption and desorption in the thin films.

DOI: 10.1021/acsaelm.9b00396
ACS Appl. Electron. Mater. 2019, 1, 1873−1880

■ ASSOCIATED CONTENT

Supporting Information

The Supporting Information is available free of charge on the ACS Publications website at DOI: 10.1021/acsaelm.9b00396.

Synthesis scheme, detailed TFT measurements, and DFT calculations (synthesis scheme, cyclic voltammetry measurement results, and TGA analysis results were reproduced from ref 36 with permission from the Royal Society of Chemistry) (PDF)

■ AUTHOR INFORMATION

Corresponding Author

*E-mail suwf@ntu.edu.tw.

ORCID

Chun-Fu Lu: 0000-0002-2520-4152

Chin-Ti Chen: 0000-0002-1493-2533

Wei-Fang Su: 0000-0002-3375-4664

Notes

The authors declare no competing financial interest.

■ ACKNOWLEDGMENTS

The authors thank the financial support from Grants MOST 107-2221-E-002-005 and MOST 106-2923-M-002-004-MY3 obtained from the Ministry of Science and Technology in Taiwan.

■ REFERENCES

(1) Broza, Y. Y.; Vishinkin, R.; Barash, O.; Nakhleh, M. K.; Haick, H. Synergy between nanomaterials and volatile organic compounds for non-invasive medical evaluation. *Chem. Soc. Rev.* **2018**, *47* (13), 4781−4859.

(2) Bajtarevic, A.; Ager, C.; Pienz, M.; Klieber, M.; Schwarz, K.; Ligor, M.; Ligor, T.; Filipiak, W.; Denz, H.; Fiegl, M.; Hilbe, W.; Weiss, W.; Lukas, P.; Jamnig, H.; Hackl, M.; Haidenberger, A.; Buszewski, B.; Miekisch, W.; Schubert, J.; Amann, A. Noninvasive detection of lung cancer by analysis of exhaled breath. *BMC Cancer* **2009**, *9*, 348.

(3) Davies, S.; Spanel, P.; Smith, D. Quantitative analysis of ammonia on the breath of patients in end-stage renal failure. *Kidney Int.* **1997**, *52* (1), 223−228.

(4) Li, H.; Shi, W.; Song, J.; Jang, H. J.; Dailey, J.; Yu, J.; Katz, H. E. Chemical and Biomolecule Sensing with Organic Field-Effect Transistors. *Chem. Rev.* **2019**, *119* (1), 3−35.

(5) Huang, W.; Besar, K.; LeCover, R.; Rule, A. M.; Breysse, P. N.; Katz, H. E. Highly sensitive NH3 detection based on organic field-effect transistors with tris(pentafluorophenyl)borane as receptor. *J. Am. Chem. Soc.* **2012**, *134* (36), 14650−14653.

(6) Yang, Y.; Zhang, G.; Luo, H.; Yao, J.; Liu, Z.; Zhang, D. Highly Sensitive Thin-Film Field-Effect Transistor Sensor for Ammonia with the DPP-Bithiophene Conjugated Polymer Entailing Thermally Cleavable tert-Butoxy Groups in the Side Chains. *ACS Appl. Mater. Interfaces* **2016**, *8* (6), 3635−3643.

(7) Nketia-Yawson, B.; Jung, A. R.; Noh, Y.; Ryu, G. S.; Tabi, G. D.; Lee, K. K.; Kim, B.; Noh, Y. Y. Highly Sensitive Flexible NH3 Sensors Based on Printed Organic Transistors with Fluorinated Conjugated Polymers. *ACS Appl. Mater. Interfaces* **2017**, *9* (8), 7322−7330.

(8) Liao, Q.; Wang, Y.; Uddin, M. A.; Chen, J.; Guo, H.; Shi, S.; Wang, Y.; Woo, H. Y.; Guo, X. Drastic Effects of Fluorination on Backbone Conformation of Head-to-Head Bithiophene-Based Polymer Semiconductors. *ACS Macro Lett.* **2018**, *7* (5), 519−524.

(9) Yang, J.; Zhao, Z.; Geng, H.; Cheng, C.; Chen, J.; Sun, Y.; Shi, L.; Yi, Y.; Shuai, Z.; Guo, Y.; Wang, S.; Liu, Y. Isoindigo-Based Polymers with Small Effective Masses for High-Mobility Ambipolar Field-Effect Transistors. *Adv. Mater.* **2017**, *29* (22), 1702115.

(10) Wang, M.; Ford, M. J.; Zhou, C.; Seifrid, M.; Nguyen, T. Q.; Bazan, G. C. Linear Conjugated Polymer Backbones Improve Alignment in Nanogroove-Assisted Organic Field-Effect Transistors. *J. Am. Chem. Soc.* **2017**, *139* (48), 17624−17631.

(11) Yum, S.; An, T. K.; Wang, X.; Lee, W.; Uddin, M. A.; Kim, Y. J.; Nguyen, T. L.; Xu, S.; Hwang, S.; Park, C. E.; Woo, H. Y. Benzotriazole-Containing Planar Conjugated Polymers with Non-covalent Conformational Locks for Thermally Stable and Efficient Polymer Field-Effect Transistors. *Chem. Mater.* **2014**, *26* (6), 2147−2154.

(12) Lu, C.-F.; Shih, C.-W.; Chen, C.-A.; Chin, A.; Su, W.-F. Tuning the Morphology of Isoindigo Donor-Acceptor Polymer Film for High Sensitivity Ammonia Sensor. *Adv. Funct. Mater.* **2018**, *28* (40), 1803145.

(13) Yu, S. H.; Cho, J.; Sim, K. M.; Ha, J. U.; Chung, D. S. Morphology-Driven High-Performance Polymer Transistor-based Ammonia Gas Sensor. *ACS Appl. Mater. Interfaces* **2016**, *8* (10), 6570−6576.

(14) Manoli, K.; Dumitru, L.; Mulla, M.; Magliulo, M.; Franco, C.; Santacroce, M.; Scamarcio, G.; Torsi, L. A comparative study of the gas sensing behavior in P3HT- and PBTTT-based OTFTs: the influence of film morphology and contact electrode position. *Sensors* **2014**, *14* (9), 16869−16880.

(15) Khim, D.; Ryu, G. S.; Park, W. T.; Kim, H.; Lee, M.; Noh, Y. Y. Precisely Controlled Ultrathin Conjugated Polymer Films for Large Area Transparent Transistors and Highly Sensitive Chemical Sensors. *Adv. Mater.* **2016**, *28* (14), 2752−2759.

(16) Huang, W.; Yu, J.; Yu, X.; Shi, W. Polymer dielectric layer functionality in organic field-effect transistor based ammonia gas sensor. *Org. Electron.* **2013**, *14* (12), 3453−3459.

(17) Puchalska, M.; Polec-Pawlak, K.; Zadrozna, I.; Hryszko, H.; Jarosz, M. Identification of indigoid dyes in natural organic pigments used in historical art objects by high-performance liquid chromatography coupled to electrospray ionization mass spectrometry. *J. Mass Spectrom.* **2004**, *39* (12), 1441−1449.

(18) Gao, Y.; Deng, Y.; Tian, H.; Zhang, J.; Yan, D.; Geng, Y.; Wang, F. Multifluorination toward High-Mobility Ambipolar and Unipolar n-Type Donor-Acceptor Conjugated Polymers Based on Isoindigo. *Adv. Mater.* **2017**, *29* (13), 1606217.

(19) Lei, T.; Cao, Y.; Zhou, X.; Peng, Y.; Bian, J.; Pei, J. Systematic Investigation of Isoindigo-Based Polymeric Field-Effect Transistors: Design Strategy and Impact of Polymer Symmetry and Backbone Curvature. *Chem. Mater.* **2012**, *24* (10), 1762−1770.

(20) Zheng, Y. Q.; Lei, T.; Dou, J. H.; Xia, X.; Wang, J. Y.; Liu, C. J.; Pei, J. Strong Electron-Deficient Polymers Lead to High Electron Mobility in Air and Their Morphology-Dependent Transport Behaviors. *Adv. Mater.* **2016**, *28* (33), 7213−7219.

(21) Mueller, C. J.; Singh, C. R.; Fried, M.; Huettner, S.; Thelakkat, M. High Bulk Electron Mobility Diketopyrrolopyrrole Copolymers with Perfluorothiophene. *Adv. Funct. Mater.* **2015**, *25* (18), 2725−2736.

(22) Fei, Z.; Boufflet, P.; Wood, S.; Wade, J.; Moriarty, J.; Gann, E.; Ratcliff, E. L.; McNeill, C. R.; Sirringhaus, H.; Kim, J. S.; Heeney, M. Influence of Backbone Fluorination in Regioregular Poly(3-alkyl-4-fluoro)thiophenes. *J. Am. Chem. Soc.* **2015**, *137* (21), 6866−6879.

(23) Zhang, A.; Xiao, C.; Wu, Y.; Li, C.; Ji, Y.; Li, L.; Hu, W.; Wang, Z.; Ma, W.; Li, W. Effect of Fluorination on Molecular Orientation of Conjugated Polymers in High Performance Field-Effect Transistors. *Macromolecules* **2016**, *49* (17), 6431−6438.

(24) Seiler, N. Ammonia and Alzheimer's disease. *Neurochem. Int.* **2002**, *41* (2), 189−207.

(25) DuBois, S.; Eng, S.; Bhattacharya, R.; Rulyak, S.; Hubbard, T.; Putnam, D.; Kearney, D. J. Breath ammonia testing for diagnosis of hepatic encephalopathy. *Dig. Dis. Sci.* **2005**, *50* (10), 1780−1784.

(26) Krishnan, S. T.; Devadhasan, J. P.; Kim, S. Recent analytical approaches to detect exhaled breath ammonia with special reference to renal patients. *Anal. Bioanal. Chem.* **2017**, *409* (1), 21−31.

DOI: 10.1021/acsaelm.9b00396
ACS Appl. Electron. Mater. 2019, 1, 1873−1880

(27) Narasimhan, L. R.; Goodman, W.; Patel, C. K. N. Correlation of breath ammonia with blood urea nitrogen and creatinine during hemodialysis. *Proc. Natl. Acad. Sci. U. S. A.* **2001**, *98* (8), 4617−4621.
(28) Kearney, D. J.; Hubbard, T.; Putnam, D. Breath ammonia measurement in Helicobacter pylori infection. *Dig. Dis. Sci.* **2002**, *47* (11), 2523−2530.
(29) Warren, J. R.; Marshall, B. Unidentified curved bacilli on gastric epithelium in active chronic gastritis. *Lancet* **1983**, *321* (8336), 1273−1275.
(30) Galassetti, P. R.; Novak, B.; Nemet, D.; Rose-Gottron, C.; Cooper, D. M.; Meinardi, S.; Newcomb, R.; Zaldivar, F.; Blake, D. R. Breath ethanol and acetone as indicators of serum glucose levels: an initial report. *Diabetes Technol. Ther.* **2005**, *7* (1), 115−123.
(31) Kim, S. J.; Choi, S. J.; Jang, J. S.; Cho, H. J.; Kim, I. D. Innovative Nanosensor for Disease Diagnosis. *Acc. Chem. Res.* **2017**, *50* (7), 1587−1596.
(32) King, J.; Kupferthaler, A.; Unterkofler, K.; Koc, H.; Teschl, S.; Teschl, G.; Miekisch, W.; Schubert, J.; Hinterhuber, H.; Amann, A. Isoprene and acetone concentration profiles during exercise on an ergometer. *J. Breath Res.* **2009**, *3* (2), 027006.
(33) Deng, C.; Zhang, J.; Yu, X.; Zhang, W.; Zhang, X. Determination of acetone in human breath by gas chromatography-mass spectrometry and solid-phase microextraction with on-fiber derivatization. *J. Chromatogr. B: Anal. Technol. Biomed. Life Sci.* **2004**, *810* (2), 269−275.
(34) Nelson, N.; Lagesson, V.; Nosratabadi, A. R.; Ludvigsson, J.; Tagesson, C. Exhaled Isoprene and Acetone in Newborn Infants and in Children with Diabetes Mellitus. *Pediatr. Res.* **1998**, *44* (3), 363−367.
(35) Khatib, M.; Huynh, T.-P.; Sun, J. J.; Do, T. T.; Sonar, P.; Hinkel, F.; Müllen, K.; Haick, H. Organic Transistor Based on Cyclopentadithiophene-Benzothiadiazole Donor-Acceptor Copolymer for the Detection and Discrimination between Multiple Structural Isomers. *Adv. Funct. Mater.* **2019**, *29*, 1808188.
(36) Liao, S.-F.; Lu, C.-F.; Fenta, A. D.; Chen, C.-T.; Chao, C.-Y.; Su, W.-F. High face-on ratio isoindigo colpolymers with extended nano-fibrillar network in fullerene-based thick (>300 nm) photovoltaics achieving high efficiency 10.7%. *J. Mater. Chem. A* **2019**, DOI: 10.1039/C9TA06719A.
(37) ASTM E104-02. Standard Practice for Maintaining Constant Relative Humidity by Means of Aqueous Solutions; ASTM International: West Conshohocken, PA, 2012.

DOI: 10.1021/acsaelm.9b00396
ACS Appl. Electron. Mater. 2019, 1, 1873−1880